PHYSICAL REVIEW D VOLUME 43, NUMBER 9 1 MAY 1991

# $\gamma$ production in $p\,^{20}$Ne and $pN$ interactions at 300 GeV

B. S. Yuldashev*
*Department of Physics, University of Washington, Seattle, Washington 98195*

Sh. M. Aliev, M. A. Alimov, Kh. Kh. Artykov, S. O. Edgorov, Sh. V. Inogamov, A. V. Khaneles,
E. A. Kosonowski, S. L. Lutpullaev, N. Rasulov, T. P. Rodionova, K. T. Turdaliev, E. Turumov, and A. A. Yuldashev
*The Physical Technical Institute, The Uzbek Academy of Sciences, Tashkent, 700084, U.S.S.R.*

R. J. Loveless and D. D. Reeder
*Department of Physics, University of Wisconsin, Madison, Wisconsin 53706*
(Received 6 August 1990)

Data on the multiplicity and inclusive spectra of $\gamma$ produced in inelastic $p\,^{20}$Ne and $pN$ interactions at 300 GeV are presented. The $\gamma$ multiplicity for $p\,^{20}$Ne interactions is $11.43\pm0.23$, and the ratio of $\langle n_\gamma \rangle$ for $p\,^{20}$Ne and $pN$ interactions is $1.48\pm0.05$. From an analysis of the effective-mass distributions, $\langle n_{\pi^0} \rangle = 4.91\pm0.52$ and $\langle n_{\eta^0} \rangle = 1.47\pm0.33$. In fact, $\eta^0$ production is much higher in $p\,^{20}$Ne interactions $[R(\eta^0/\pi^0)=0.66\pm0.12$ for $n_p \geq 2]$ than in $pN$ interactions $[R(\eta^0/\pi^0)=0.06\pm0.04]$. No $\eta'(958)$ signal is seen. Strong correlations between $\langle n_\gamma \rangle$ and $n_p$, the number of secondary protons, are observed, primarily from the central and target fragmentation regions. Inclusive $y^*$ and $p_\perp$ spectra are analyzed and evidence for low-energy cascading and rescattering of fast particles in the projectile fragmentation region is discussed. The data are compared to the predictions of the additive quark model, the Lund model, and the dual parton model.

## I. INTRODUCTION

Many of the main features of hadron-nucleus ($hA$) and hadron-nucleon ($hN$) inelastic interactions have been learned from the study of the production of charged particles. However, there are only a few experiments (particularly true for nuclear targets) in which data for both charged and neutral hadrons are available. The importance of such experiments is clear when one considers that neutral particles constitute at least 30% of secondary hadrons.

This experiment presents data on $\gamma$ inclusive production in $p\,^{20}$Ne and $pN$ ($pp,pn$) interactions at 300 GeV/$c$. These inclusive $\gamma$ come, of course, almost exclusively from $\pi^0$ and $\eta^0$ decays. Hence, this experiment can make detailed measurements of both $\pi^0$ and $\eta^0$ production from neon and from single nucleons.

These data are compared to predictions of the additive quark model[1] (AQM), the Lund model (version FRITIOF-2)[2] (LM) and the dual parton model[3] (DPM) according to Ref. 4. Although these models were developed to describe soft $hA$ and $hN$ interactions, the contribution of low-energy cascading is taken into account only in the AQM, in which low-energy hadrons formed from low-$x$ partons in a nucleus can interact. We emphasize that these models incorporate different pictures of the nucleus. For example, in the LM and the DPM, all nucleons in the nucleus are distributed according to conventional parametrizations of nuclear density (Gaussian, Fermi, or Woods-Saxon functions), whereas the AQM assumes, in addition, that the projectile hadron (or secondary hadrons) can interact with correlated pairs of nucleons in a nucleus.[5] Also, in the LM and the DPM, the production of hadrons from all $SU_3$ multiplets are taken into account (with relevant cross sections), whereas in the AQM only nucleons, pions, $\Delta$ isobars, and vector mesons ($\rho,\omega$) are considered. For each model we have generated, by a Monte Carlo technique, more than 20 000 events of each type ($p\,^{20}$Ne, $pp$, $pn$) of interaction.

## II. EXPERIMENTAL PROCEDURE

The data come from an exposure of the 30-in. Fermilab bubble chamber to a diffractive proton beam of momentum 300 GeV/$c$.[6] The bubble chamber was filled with a light neon-hydrogen mixture [$(30.9\pm0.7)$% molar Ne]. The density and the radiation length of this mixture are 0.249 g/cm$^3$ and 128.1 cm, respectively.

The results presented in this paper were obtained from triple scanning 26 024 frames where approximately 9000 primary interactions were found. The events were classified as "$p$ Ne," "$pp$" and "$pn$" interactions in accordance with a standard procedure of event selection in bubble-chamber experiments with heavy mixtures (see Ref. 6). In a further analysis, the correct number of $p\,^{20}$Ne interactions was determined statistically on the basis of measured cross sections of $p\,^{20}$Ne and $pp$ interactions at 300 GeV and of the number of events classified in scanning as "neonic" and "hydrogenic" (details of this procedure are described in Ref. 6). In each primary interaction the number of secondary charged particles, negatively charged hadrons ($\simeq 95$% are $\pi^-$ mesons), and protons were determined. The protons were identified by ionization and range; after momentum measurement, only protons with momenta of $0.12 \le p_p \le 1.2$ GeV/$c$ were retained for further analysis.

A $\gamma$ is recorded by an $e^+e^-$ conversion pair in the visible volume of the bubble chamber. The identification of fast $\gamma$ and neutral strange particles ($V^0$), which decayed downstream in the bubble chamber, was done after momentum measurements and kinematical analysis (see below). All recorded events containing $\gamma$ and $V^0$ were measured and processed through geometrical reconstruction and kinematical analysis programs. Because of the relatively high multiplicity of charged secondaries in some events, it was difficult to accurately measure the vertex of a $\gamma$ (or $V^0$) which converted (decayed) within 1.5 cm of the primary vertex. As a result, only $\gamma$ and $V^0$ with distance $l \ge 2$ cm were retained for further analysis.

The fast $\gamma$ and $V^0$ were distinguished using the transverse momentum $p_\perp$ of negative particles ($e^-$, $\pi^-$, or $\bar{p}$) produced from a $\gamma$ conversion or $V^0$ decay ($K_S^0$, $\Lambda^0$, $\bar{\Lambda}^0$). $\gamma$ conversions were selected to be those with $p_\perp^{(-)} < 20$ MeV/$c$. The contamination of fast $V^0$ having $p_\perp^{(-)} < 20$ MeV/$c$, i.e., simulating a $\gamma$, is less than 1.3%.

After the identification of $\gamma$ and a fiducial-volume selection, 8153 primary events with 5964 $\gamma$ remained. The geometrical weight for each measured $\gamma$ was determined to be

$$W_g = \left[ \exp\left[ -\frac{\mu(E_\gamma)L_{\min}}{x_0} \right] - \exp\left[ -\frac{\mu(E_\gamma)L_{\rm pot}}{x_0} \right] \right]^{-1}, \quad (1)$$

where $L_{\min} = 2$ cm, $L_{\rm pot}$ is the potential length of $\gamma$ in the given fiducial volume, $x_0 = 128.1$ cm is the radiation length of the $NeH_2$ mixture, and $\mu(E_\gamma)$ is the energy-dependent $\gamma$-conversion coefficient. The average $W_g$ is found to be $\langle W_g \rangle = 8.72 \pm 0.11$.

Corrections were also made for (a) the loss of low-energy ($p_\gamma \le 40$ MeV/$c$) $\gamma$ due to the geometrical reconstruction failure of low-energy $e^\pm$ tracks and the consequent low efficiency of detecting such a $\gamma$, (b) energetic $\gamma$ which convert within the narrow ($\theta_{\rm lab} \le 5°$) forward cone of the fast, charged hadrons and are thus unmeasurable, and (c) the loss of $\gamma$ emitted nearly along the magnetic field.

The correction for low-energy $\gamma$ was done using the Peyrou plot (a plot of transverse versus longitudinal momentum) for $\gamma$ having $p_\perp < 0.1$ GeV/$c$ in the laboratory system. This two-dimensional plot for $\gamma$ should be symmetric relative to the $p_\parallel^* = 0$ axis in the center of mass of $pp$ interactions. We observe that the $\gamma$ multiplicity rises 14.7% for $\gamma$ tracks with $p_{\rm lab} < 0.040$ GeV/$c$.

The correction for unmeasured, fast $\gamma$ was made using an analysis of the $\gamma$ angular distribution in the center-of-mass frame for events classified as $pp$ events. As one can see from Fig. 1, there is a forward-backward asymmetry for $\gamma$ at $|\cos\theta^*| \ge 0.8$ which is due mainly to the failure of $\gamma$-vertex reconstruction for those $\gamma$ which converted in the narrow ($\theta_{\rm lab} \le 5°$) cone of charged secondaries and to those $\gamma$ which converted close ($\lesssim 15$ cm) to the end of the fiducial volume. The latter circumstance makes it difficult to reconstruct, with a good accuracy, those $e^\pm$ tracks with momenta $p_{e^\pm} \gtrsim 40$ GeV/$c$. In order to correct for this loss, we have introduced a weight factor for $\gamma$ with $\cos\theta^* > 0.8$:

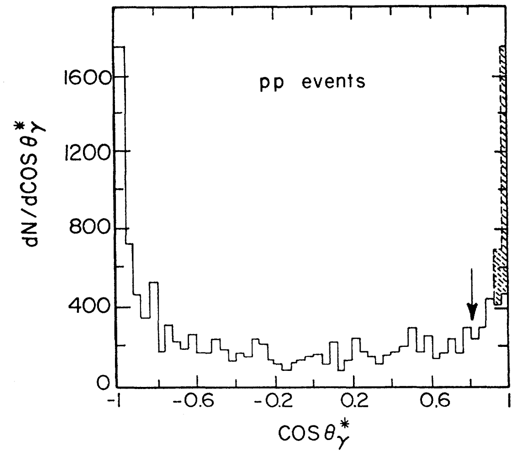


FIG. 1. The $\gamma$ angular distribution in the center-of-mass system (c.m.s.) of $pp$ interactions. Corrections for unmeasured fast $\gamma$ are shown in the dashed area. The arrow indicates the region ($\cos\theta^* > 0.8$) in which a weighting factor was introduced to correct for missing $\gamma$.

$$k_i(\cos\theta_\gamma^*) = \frac{\sum W_\gamma^*(-\cos\theta_{\max}^* < \cos\theta_\gamma^* < -\cos\theta_{\min}^*)}{\sum W_\gamma^*(\cos\theta_{\min}^* < \cos\theta_\gamma^* < \cos\theta_{\max}^*)} \quad (2)$$

for symmetric intervals of $\cos\theta_\gamma^*$. The corrections were made for four symmetric intervals: $i = 1$ has $0.95 \le \cos\theta^* \le 1.00$, $i = 2$ has $0.90 \le \cos\theta \le 0.95$, $i = 3$ has $0.85 \le \cos\theta^* \le 0.90$, and $i = 4$ has $0.80 \le \cos\theta^* \le 0.85$. In this procedure we also took into account the dependence of $k_i(\cos\theta_\gamma^*)$ on the multiplicity of charged secondaries in the event. For example, for $pp$ events with $n_{\rm ch} \le 8$, the average value of $k(\cos\theta_\gamma^*)$ is found to be 1.07, whereas for $pp$ events with $n_{\rm ch} > 10$ this value is 1.51. For $p\,^{20}$Ne and $pn$ events, we assumed the corrections were identical to those for $pp$ events.

Correction for the loss of $\gamma$ emitted along the magnetic field $k_\varphi$ was made by assuming isotropy in the azimuthal plane.

Finally, for each $\gamma$ the weight obtained by combining these corrections is

$$W_\gamma = W_g k_\varphi k_i(\cos\theta^*) . \quad (3)$$

The distribution of $\gamma$ weights $W_\gamma$ is shown in Fig. 2 as a function of the $\gamma$ momentum. The average weight is $\langle W_\gamma \rangle = 12.20 \pm 0.15$.

The average error in momentum and angle measurement of the $\gamma$ are found to be $\langle \delta p/p \rangle = 14.5\%$, $\langle \delta \tan\alpha \rangle = 0.03$, and $\langle \beta \rangle = 0.004$ rad, where $\alpha$ and $\beta$ are the dip and azimuthal angles, respectively. We have excluded from this analysis all identified bremstrahlung $\gamma$'s. More details concerning this analysis can be found in Refs. 7 and 8.

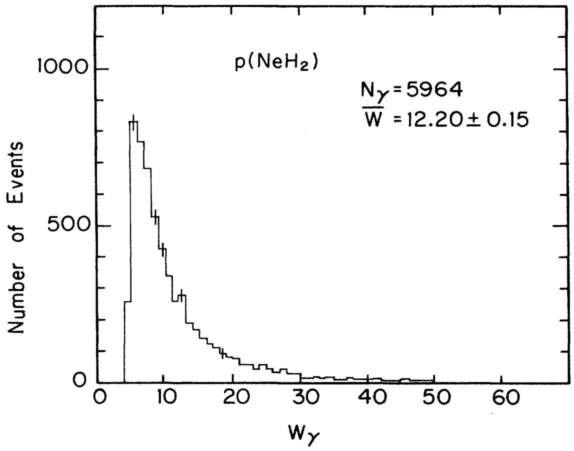


FIG. 2. The distribution of $\gamma$ weights $W_\gamma$ for the entire sample of measured $\gamma$.

## III. AVERAGE $\gamma$ MULTIPLICITY

The average $\gamma$ multiplicity was determined from the expression

$$\langle n_\gamma \rangle = \frac{\sum W_\gamma}{N_0} , \quad (4)$$

where $W_\gamma$ is the $\gamma$ weight and $N_0$ is the number of interactions of a given type ($p\,^{20}$Ne, $pp$, or $pn$). We removed coherent $p\,^{20}$Ne events and elastic $pp$ interactions. This was done statistically based on known cross sections.[6]

The experimental values of $\langle n_\gamma \rangle$ are given in Table I. We note that our data for $pp$ interactions are consistent with measurements of $\langle n_\gamma \rangle_{pp}$ in hydrogen bubble chambers at 300 GeV/$c$.[9,10]

Also in Table I are the multiplicities expected from Monte Carlo calculations using the various nuclear models AQM,[1] LM,[2] and DPM.[4] Within (5–10)%, all models are in agreement with our experimental results. Also shown in Table I are the results of the $\langle n_\gamma \rangle$ calculations for $p\,^{20}$Ne interactions in the framework of the intranuclear cascading model[11] (ICM) which overestimates the average multiplicity of $\gamma$'s.

The ratio of the average $\gamma$ multiplicity produced in $p\,^{20}$Ne and $pN$ (averaged over $pp$ and $pn$ events) is

$$R(\gamma) = \frac{\langle n_\gamma(p\,^{20}\mathrm{Ne}) \rangle}{0.5[\langle n_\gamma(pp) \rangle + \langle n_\gamma(pn) \rangle]} = 1.48 \pm 0.05 . \quad (5)$$

This number is consistent with $R(n_-)=1.47\pm0.03$ obtained by us for negative particles in $p\,^{20}$Ne and $pN$ interactions at 300 GeV.[6]

## IV. $\gamma$ SOURCES

In hadronic reactions with nuclei and nucleons the main sources of secondary $\gamma$ are the decays of well-known hadrons:[12]

$$\begin{aligned}
&\pi^0 \to \gamma\gamma, \quad B=98.8\% , \\
&\eta^0(549) \to \gamma\gamma, \quad B=38.9\% , \\
&\eta'(958) \to \gamma\gamma, \quad B=2.2\% , \\
&\qquad\quad\; \to \rho^0\gamma, \quad B=30.1\% , \\
&\qquad\quad\; \to \omega^0\gamma, \quad B=3.0\% , \\
&\omega^0(783) \to \pi^0\gamma, \quad B=8.0\% , \\
&\Sigma^0(1193) \to \Lambda^0\gamma, \quad B=100\% ,
\end{aligned} \quad (6)$$

where $B$ is the branching ratio of the given decay mode. We neglect production from charm and $b$-flavor hadrons because the production cross section is much smaller than the listed hadrons.

Experimental measurements of the production cross sections of these hadrons are important in order to analyze the predictions of different models of $hA$ and $hN$ interactions. For example, it is interesting to measure relative yields of $\pi^0$, $\eta^0$, and $\eta'(958)$ mesons because of the different quark composition of these mesons. Recent observation of an anomalously high cross section for $\eta'(958)$ production in $\pi^- p$ interactions at 360 GeV/$c$ (Ref. 13) requires a serious inspection of different models.[14]

Moreover, the determination of all possible sources of $\gamma$'s is also important from the point of view of production of direct photons[15,16] which can originate from the quantum chromodynamics (QCD) gluon Compton scattering ($qg \to q\gamma$), $q\bar{q}$ annihilation ($q\bar{q} \to q\gamma$), or gluon bremstrahlung.

In this paper we have analyzed the effective-mass spectra of $\gamma\gamma$ pairs and other $\gamma$ combinations in order to determine possible $\gamma$ sources in $p\,^{20}$Ne and $pN$ interactions. Data for $pp$ and $pn$ interactions were combined due to limited statistics.

In Fig. 3 the effective-mass spectra of $\gamma\gamma$ pairs in $p\,^{20}$Ne and $pN$ events containing at least two recorded $\gamma$ conversions in the final state are shown. There are clear peaks at the $\pi^0$ mass in both the $p\,^{20}$Ne and $pN$ interactions. For $p\,^{20}$Ne events there is also an excess of 4327

TABLE I. The average $\gamma$ multiplicity for incoherent $p\,^{20}$Ne and inelastic $pp$ and $pn$ interactions at 300 GeV/$c$ and the Monte Carlo predictions.

| Type of interaction | Experiment | AWM (Ref. 1) | LM (Ref. 2) | DPM (Ref. 4) | ICM (Ref. 11) |
|---|---|---|---|---|---|
| $p\,^{20}$Ne | 11.43±0.23 | 10.77 | 12.07 | 11.55 | 12.84 |
| $pp$ | 7.93±0.18 | | 7.84 | 8.11 | |
| $pn$ | 7.61±0.35 | | 7.77 | 8.22 | |

weighted events at the $\eta^0(549)$ mass region.

The experimental distributions for $M(\gamma\gamma)(\equiv\mu)$ were fitted to the form

$$F(\mu)=\alpha G_{\pi^0}(\mu)+\beta G_{\eta^0}(\mu)+\gamma B(\mu)\ , \tag{7}$$

where $G_{\pi^0}(\mu)$ and $G_{\eta^0}(\mu)$ are Gaussian distributions in which the known masses of $\pi^0$ and $\eta^0$ mesons are used. The widths of these Gaussians were determined by the experimental resolution in $M(\gamma\gamma)$, which is shown in Fig. 3(c) as a function of $M(\gamma\gamma)$. The function $B(\mu)$, which parametrizes the background contribution, was chosen to be of the form

$$B(\mu)=\mu^{a_1}\exp[-(a_2+a_3\mu+a_4\mu^2+a_5\mu^3)]\ . \tag{8}$$

A second method of estimating background is to randomly mix $\gamma$ from different events. This was done for each of the spectra presented; both methods gave similar results. For established $\gamma\gamma$ peaks we have represented the background with the fit; where the peak is less clear we have used randomly mixed backgrounds.

From the fit of data in Figs. 3(a) and 3(b) to Eq. (7), we have obtained for the $\eta^0/\pi^0$ ratios:

$$R(\eta^0/\pi^0)_{p\,\mathrm{Ne}}=0.29\pm0.07\ ,$$

$$\chi^2/N_{\mathrm{DF}}=0.65 \quad \text{for } p\,^{20}\mathrm{Ne} \text{ interactions}$$

and

$$R(\eta^0/\pi^0)_{pN}=0.05\pm0.04\ ,$$

$$\chi^2/N_{\mathrm{DF}}=0.51 \quad \text{in } pN \text{ events}\ .$$

The latter result is consistent with measurements of the $\eta^0/\pi^0$ ratio in the low-$p_\perp$ region ($0.2\leq p_\perp\leq1.5$ GeV/$c$) for $pp$ interactions at $\sqrt{s_{pp}}=63$ GeV/$c^2$.[17]

In order to reduce the combinatorial background, one

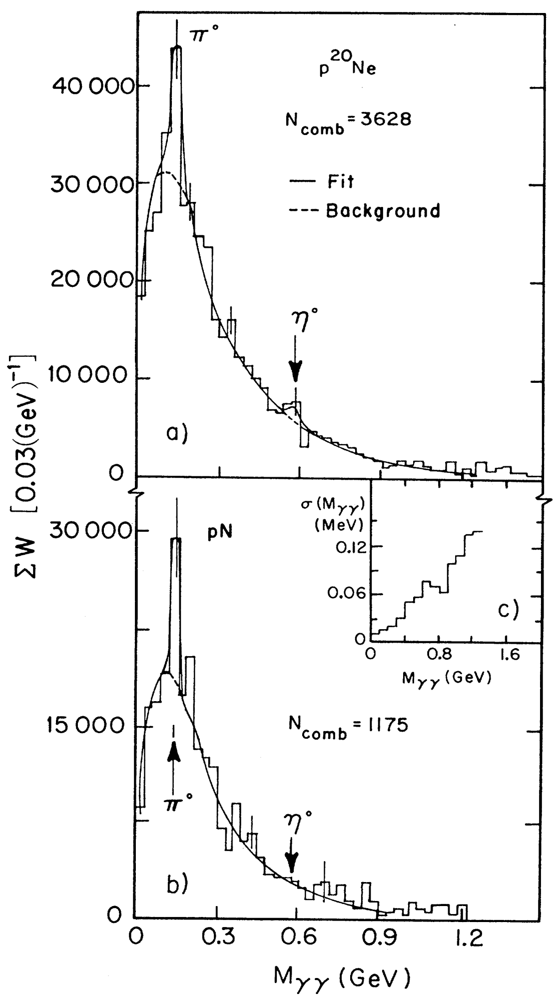


FIG. 3. The effective-mass distributions of $\gamma\gamma$ pairs in the (a) $p\,^{20}$Ne and (b) $pN$ interactions. The solid lines are the results of a fit to Eq. (7); the dashed curves correspond to the estimated background according to Eq. (8). In (c) the experimental $\gamma\gamma$-mass resolution is shown as a function of $M(\gamma\gamma)$.

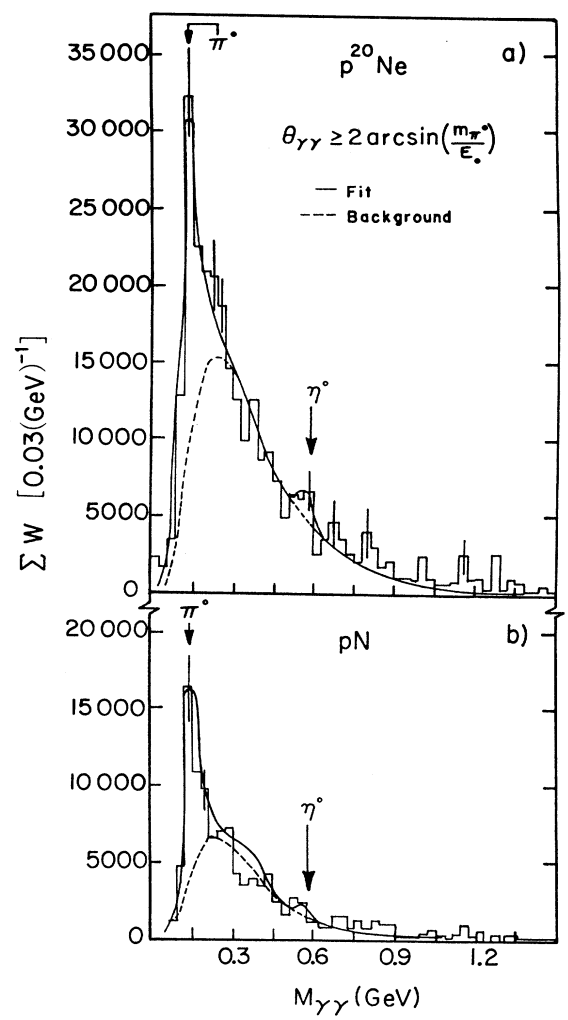


FIG. 4. $M(\gamma\gamma)$ distributions for $\gamma$ pairs satisfying the condition $\theta_{\gamma\gamma}\geq2\arcsin(m_{\pi^0}/E_0)$ for the (a) $p\,^{20}$Ne and (b) $pN$ interactions. Solid and dashed curves are fits to expected signal [Eq. (7)] and background [Eq. (8)], respectively.

can use the kinematical constraint for the minimum opening angle between two $\gamma$'s produced from the decay of a particle with mass $m_0$ having energy $E_0$:

$$\theta_{\gamma\gamma}^{\min} \geq 2\arcsin(m_0/E_0) \ . \tag{9}$$

We have used expression (9) assuming that $E_0$ equals the sum of the energies of two $\gamma$'s and $m_0 = m_{\pi^0}$. The $M(\gamma\gamma)$ spectra obtained under these assumptions in $p\,^{20}$Ne and $pN$ interactions are shown in Figs. 4(a) and 4(b). The solid lines represent the results of a fit to expression (7). For this case we find

$$R(\eta^0/\pi^0)_{p\,\mathrm{Ne}} = 0.36 \pm 0.05$$

in $p\,^{20}$Ne interactions

and

$$R(\eta^0/\pi^0)_{pN} = 0.06 \pm 0.04 \quad \text{in } pN \text{ events} \ .$$

The dashed curves show a contribution of fitted background.

We emphasize that the signal from $\eta^0$ production can be seen even more clearly by substituting the $\eta^0$ mass into expression (9) instead of $m_{\pi^0}$. This reduces the background in the region of the $\eta^0$ as seen in Fig. 5. The solid lines in Figs. 5(a) and 5(b) represent fits to the sum of a Gaussian function centered on $m_{\eta^0}$ and the background contribution from Eq. (8).

The $\eta^0/\pi^0$ ratio is clearly greater in the $p\,^{20}$Ne interactions than in the $pN$ events. This difference arises mainly in the $p\,^{20}$Ne events with at least two identified protons ($0.12 \leq p_p \leq 1.2$ GeV/$c$) in the final state. For example, in Fig. 6 we show the $M(\gamma\gamma)$ distributions for $p\,^{20}$Ne interactions with $n_p \geq 2$; the $\eta^0$ signal in this case is much stronger than the corresponding $\eta^2$ signal in Fig. 3(a). From a fit of the data in Fig. 6 to Eq. (7) we have obtained

$$R(\eta^0/\pi^0)_{p\,\mathrm{Ne},\,n_p \geq 2} = 0.66 \pm 0.12 \ .$$

In addition, from Figs. 7(a) and 7(b) one can see that the signal from $\eta^0$ production is significantly larger in the $p\,^{20}$Ne interactions with $n_p \geq 2$ than for $n_p \leq 1$, where the $\eta^0/\pi^0$ ratio is consistent with zero ($\eta^0/\pi^0 = 0.04 \pm 0.06$). The latter includes mostly interactions with quasifree nucleons of neon (see Ref. 6), and would be expected to be similar to the $pN$ interactions.

If one takes into account that the number of secondary protons in $hA$ interactions can serve as a measure of the average number of target nucleons $\langle \nu \rangle$ involved in $hA$ collisions,[6,18–20] the $\eta^0/\pi^0$ ratio for the $p\,^{20}$Ne interactions with $n_p \geq 2$ implies a strong $A$ dependence in $\eta^0$ production because $\langle \nu \rangle \simeq A^{1/3}$. On the other hand, since the quark composition of the $\eta^0$ meson

$$|\eta^0\rangle = \frac{|u\bar{u}\rangle + |d\bar{d}\rangle - 2|s\bar{s}\rangle}{\sqrt{6}}$$

includes $s\bar{s}$ quarks, the higher ratio on a nuclear target (compared to a nucleon) may indicate that sea quarks play a more important role in the nucleus.

We have also looked for the $\eta'(958)$ meson. In Fig. 8

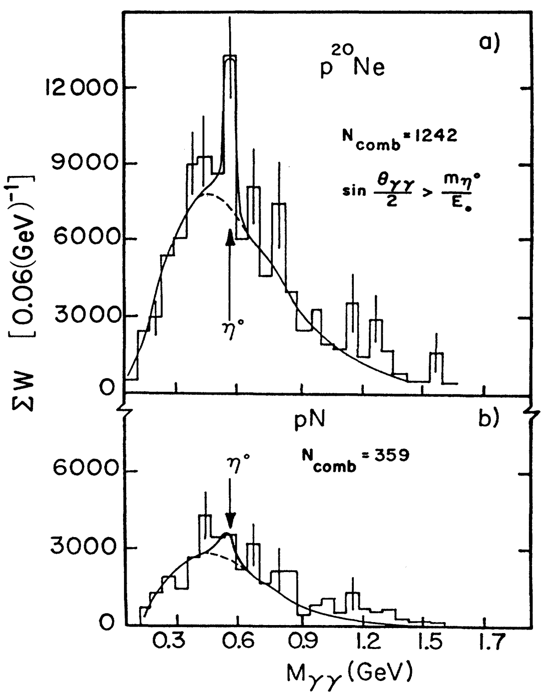


FIG. 5. $M(\gamma\gamma)$ distributions for $\gamma$ pairs with $\theta_{\gamma\gamma} > 2\arcsin(m_{\eta^0}/E_0)$ in the (a) $p\,^{20}$Ne and (b) $pN$ interactions. The solid curve is a fit to the sum of the background (dashed line) and a Gaussian function for the expected mass of the $\eta^0$.

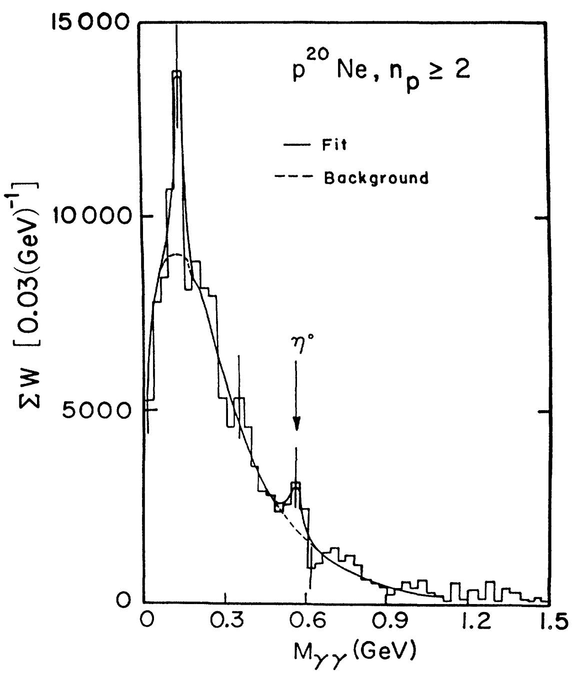


FIG. 6. $M(\gamma\gamma)$ spectrum for $p\,^{20}$Ne interactions with $n_p \geq 2$. The solid line is a fit to Eq. (7); the dashed curve is a fitted background from Eq. (8).

the $M(\gamma\gamma)$ spectrum for $p\,^{20}$Ne interactions is shown where we have used the kinematical constraint [Eq. (9)] with $m_0 = m_{\eta'}$. The solid line represents a random background obtained by mixing $\gamma$'s from different events and normalizing to the experimental area. There is no clear signal exceeding the background at $M(\gamma\gamma) \simeq m_{\eta'}$. If we take into account the experimental resolution in $M(\gamma\gamma)$, then the upper limit for the ratio $\eta'(958)/\eta^0(549)$ becomes (90% C.L.):

$$\eta'(958)/\eta(549) < 0.58 \quad \text{in } p\,^{20}\text{Ne interactions} .$$

Another possible source of $\gamma$ conversions are decays of $\Sigma^0$ hyperons. In order to search for $\Sigma^0$ we have used results from the measurements of neutral strange particles[20] and selected events containing at least one identified $\Lambda^0$ hyperon and one $\gamma$. The geometrical efficiency for recording $\Lambda^0$ decays was corrected, as were other sources of losses. The data were fitted to a Gaussian with a polynomial background. The average $\gamma$ multiplicity produced from $\Sigma^0 \to \Lambda^0\gamma$ decays is $\langle n_\gamma \rangle_\Sigma = 0.074 \pm 0.017$, which is $(0.65 \pm 0.16)\%$ of all secondary $\gamma$ in $p\,^{20}$Ne interactions at 300 GeV. A similar procedure carried out for $pN$ interactions leads to $\langle n_\gamma \rangle_\Sigma = 0.05 \pm 0.03$, or $(0.6 \pm 0.4)\%$ of all $\gamma$.

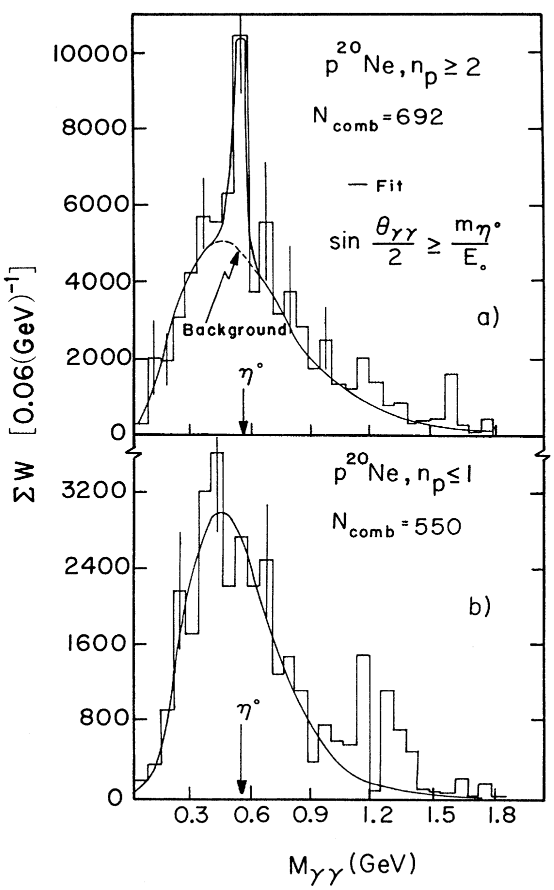


FIG. 7. $M(\gamma\gamma)$ distributions for $\gamma$ pairs with $\theta_{\gamma\gamma} > 2\arcsin(m_{\eta^0}/E_0)$ for $p\,^{20}$Ne events with the number of protons (a) $n_p \geq 2$ and (b) $n_p \leq 1$. The $\eta^0$ signal is more pronounced in (a) than in (b), where it is consistent with zero.

From an analysis of $\pi^0\gamma$ spectra looking for the decay $\omega^0 \to \pi^0\gamma$, we find the $\omega^0$ multiplicity $\langle n_{\omega^0} \rangle \leq 1.5$ with 95% C.L. Since the branching ratio for this decay is only $(8.0 \pm 0.9)\%$,[12] we expect only a few such decays, and thus have little sensitivity for this reaction.

From measurements of the ratio $\eta^0/\pi^0$ and the average $\gamma$ multiplicity, one can derive the multiplicity for $\pi^0$ and $\eta^0$ mesons using the expressions

$$\langle n(\pi^0) \rangle = \frac{\langle n_\gamma \rangle - \langle n_\gamma \rangle_\Sigma}{2(1+BR)} , \tag{10}$$

$$\langle n(\eta^0) \rangle = R \langle n(\pi^0) \rangle , \tag{11}$$

where $\langle n_\gamma \rangle$ is the average multiplicity for all $\gamma$, $\langle n_\gamma \rangle_\Sigma$ the multiplicity for $\Sigma^0 \to \Lambda^0\gamma$ decay, $R$ is the measured ratio of $\eta^0$ to $\pi^0$, and $B = 0.39$ is the branching ratio for $\eta^0 \to \gamma\gamma$ decay.

From our data we have obtained

$$\langle n(\pi^0) \rangle_{p\,\mathrm{Ne}} = 4.91 \pm 0.52 ,$$

$$\langle n(\eta^0) \rangle_{p\,\mathrm{Ne}} = 1.47 \pm 0.33 \quad \text{in } p\,^{20}\text{Ne interactions}$$

and

$$\langle n(\pi^0) \rangle_{pN} = 3.82 \pm 0.41 ,$$

$$\langle n(\eta^0) \rangle_{pN} = 0.23 \pm 0.15 \quad \text{in } pN \text{ events} .$$

When one takes into account the probability of $\eta^0 \to \gamma\gamma$ decays, we conclude that, in $p\,^{20}$Ne interactions,

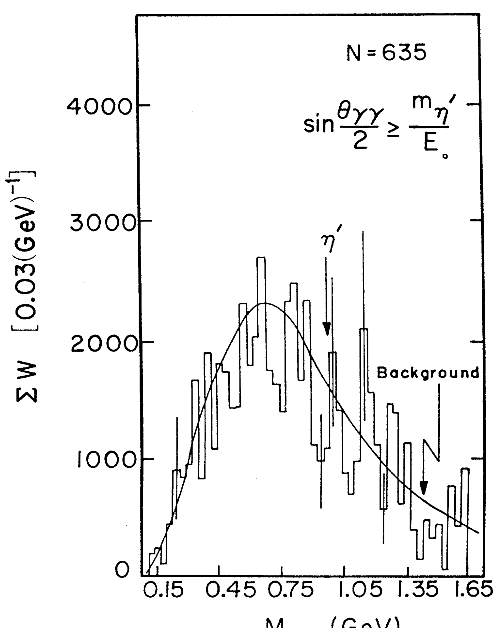


FIG. 8. The $M(\gamma\gamma)$ spectrum for $\gamma$ pairs with $\theta_{\gamma\gamma} > 2\arcsin(m_{\eta'}/E_0)$ in the $p\,^{20}$Ne interactions. The curve is a random background obtained by mixing $\gamma$'s from different events.

less than 0.5% of secondary recorded $\gamma$'s can be attributed to sources other than $\pi^0$, $\eta^0$, and $\Sigma^0$ decays.

## V. MULTIPLICITY CORRELATIONS

A study of the correlations between the multiplicities of neutral and charged hadrons can reveal some dynamical aspects of multiparticle production. In this paper we have investigated correlations between the average multiplicities of secondary $\gamma$'s and charged particles (pions and protons) in $p\,^{20}$Ne and $pN$ interactions.

In Fig. 9 the dependence of $\langle n_\gamma \rangle$ on the number $n_-$ of negative hadrons ($\simeq 95\%$ of them are $\pi^-$ mesons) in $p\,^{20}$Ne and $pN$ interactions is shown. In both types of interaction $\langle n_\gamma \rangle$, the mean $\gamma$ multiplicity increases approximately linearly with $n_-$ until $n_- \approx 10-11$. Using a linear fit $\langle n_\gamma \rangle = \alpha + \beta n_-$, we find (for $n_- \leq 10$)

$$\alpha_{p\,\mathrm{Ne}} = 4.96 \pm 0.49, \quad \beta_{p\,\mathrm{Ne}} = 1.27 \pm 0.10 \quad (\chi^2/N_{\mathrm{DF}} = 1.15) \text{ for } p\,^{20}\mathrm{Ne} \text{ interactions}$$

and

$$\alpha_{pN} = 3.12 \pm 0.28, \quad \beta_{pN} = 1.40 \pm 0.09 \quad (\chi^2/N_{\mathrm{DF}} = 1.22) \text{ for } pN \text{ events .}$$

Thus, the slope parameter $\beta$ depends weakly on the type of target, which may be a reflection of isospin and charge conservation.

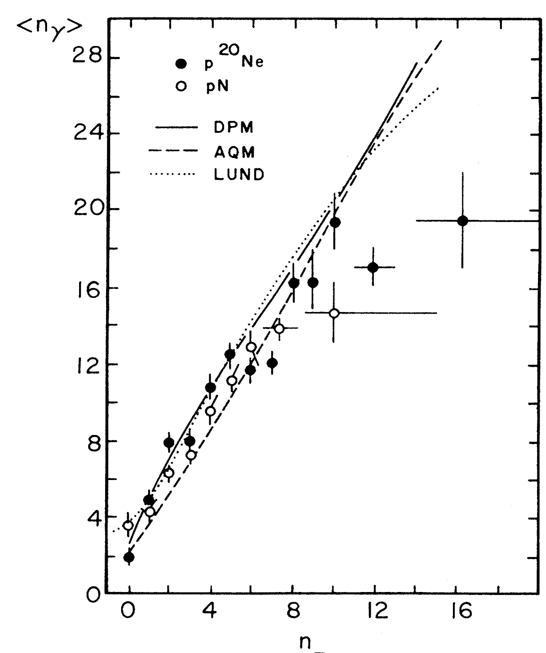


FIG. 9. The average $\gamma$ multiplicity as a function of the number of negative particles ($n_-$) for $p\,^{20}$Ne and $pN$ interactions. The curves show the predictions of different models for $p\,^{20}$Ne interactions: the additive quark model (AQM), the Lund model (LM), and the dual parton model (DPM).

The curves shown in Fig. 9 are the model predictions for the AQM, LM, and DPM for $p\,^{20}$Ne interactions. Within $\sim$(10–20)%, all these models are in agreement with experiment for $n_- \lesssim 10-11$. Since events with $n_- > 10$ constitute less than 9% of the total inelastic cross section, the bulk of the data is well described by these models.

This correlation between $\langle n_\gamma \rangle$ and $n_-$ originates from hadrons produced in both the central and the target-fragmentation regions. This effect is demonstrated in Fig. 10 where we show the correlation for three different rapidity intervals ($y^* < -1$, $|y^*| \leq 1$, and $y^* > 1$) for $p\,^{20}$Ne and $pN$ interactions. The correlations are quite weak for $y^* > 1$, i.e., for those $\gamma$ produced from decays of $\pi^0(\eta^0)$ mesons which originate primarily in the projectile-fragmentation region. Again, the disagreement between the data and the various model calculations occurs mainly at large values of $n_-$.

The multiplicity of secondary protons in nuclear interactions can serve as a measure of the average number of nucleons involved in the $hA$ interaction.[6,18–20] Hence, the correlation of $\langle n_\gamma \rangle$ and the number of protons in the

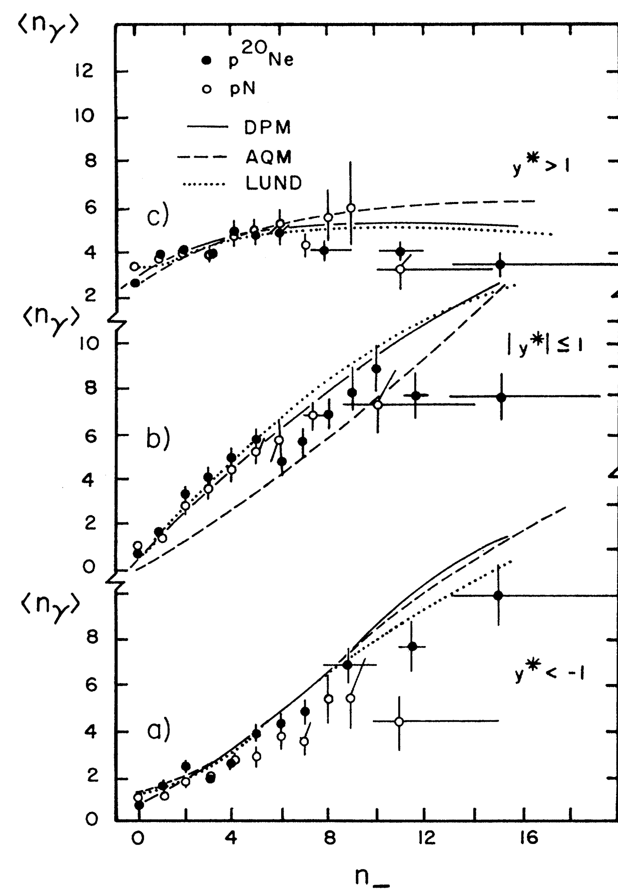


FIG. 10. The dependence of $\langle n_\gamma \rangle$ on $n_-$ for $\gamma$ with rapidity (a) $y^* < -1$ (b) $|y^*| \leq 1$, and (c) $y^* > 1$ for $p\,^{20}$Ne and $pN$ interactions. The curves correspond to the predictions of the corresponding models.

final state is a critical test of the predictive power of the various models. in Fig. 11 ($p\,^{20}$Ne interactions) we see that, although AQM, LM, and DPM all satisfactorily describe the $\langle n_\gamma \rangle = f(n_-)$ correlations, there are substantial differences among these models in the correlation predictions for $\langle n_\gamma \rangle$ and $n_p$, the number of protons identified in the final state. For example, the LM contradicts the data, while the DPM agrees with data for larger-momentum ($0.4 \le p_p \le 1.2$ GeV/$c$) protons. One reason for this discrepancy is that, in experimental spectra for protons with momenta of $0.12 \le p \le 1.20$ GeV/$c$, there are contributions from three mechanisms:[21] "evaporated" protons, knocked-out protons, and cumulative protons. In both the LM and the DPM, all secondary protons are assumed to be knocked-out nucleons. The AQM, in addition to these protons, assumes that secondary protons can be produced by the interaction of hadrons with correlated pairs of nucleons in a nucleus.[5]

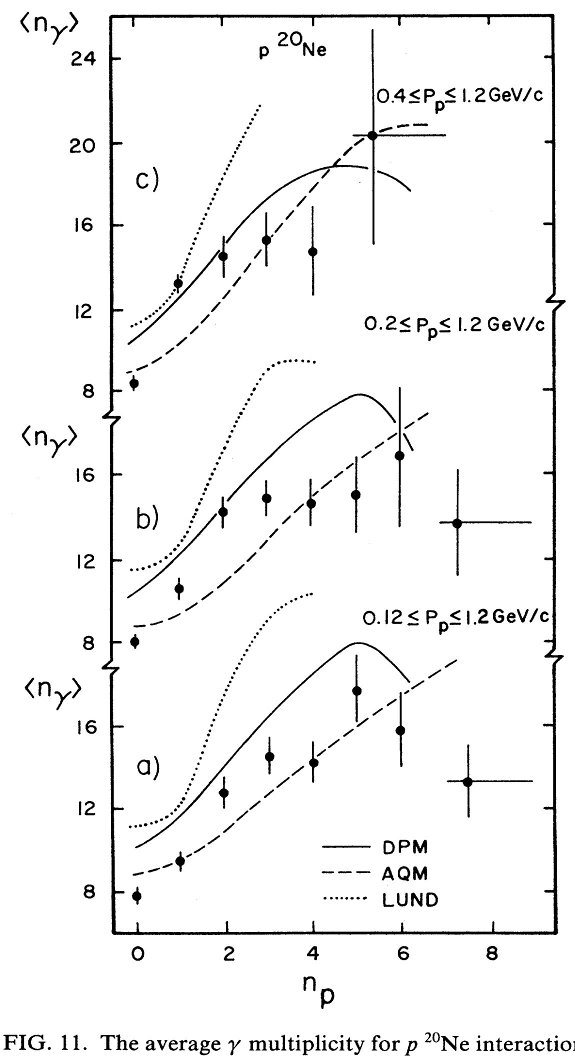


FIG. 11. The average $\gamma$ multiplicity for $p\,^{20}$Ne interactions as a function of the number of protons $n_p$ with momenta: (a) $0.12 \le p_p \le 1.2$ GeV/$c$, (b) $0.2 \le p_p \le 1.2$ GeV/$c$, and (c) $0.4 \le p_p \le 1.2$ GeV/$c$. The curves are predictions of the discussed models.

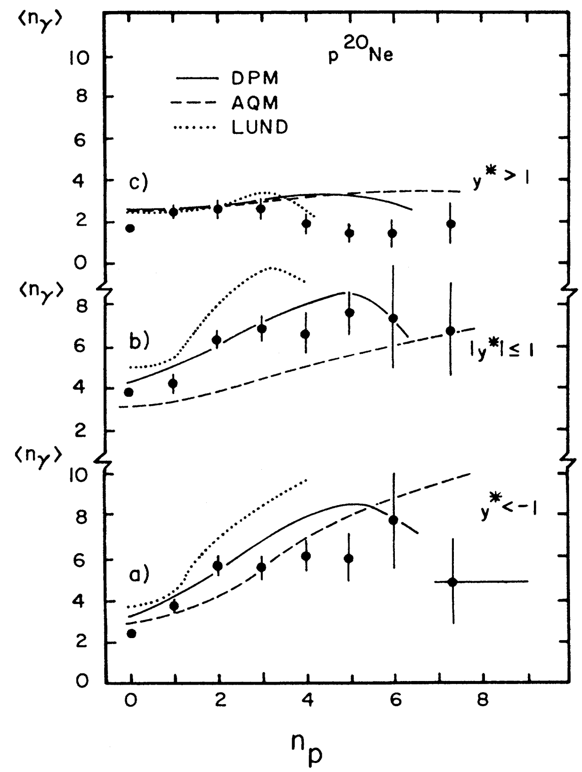


FIG. 12. The dependence of $\langle n_\gamma \rangle$ on the number of protons with momenta $0.12 \le p_p \le 1.20$ GeV/$c$ for $p\,^{20}$Ne interactions for $\gamma$ with rapidity: (a) $y^* < -1$, (b) $|y^*| \le 1$, and (c) $y^* > 1$.

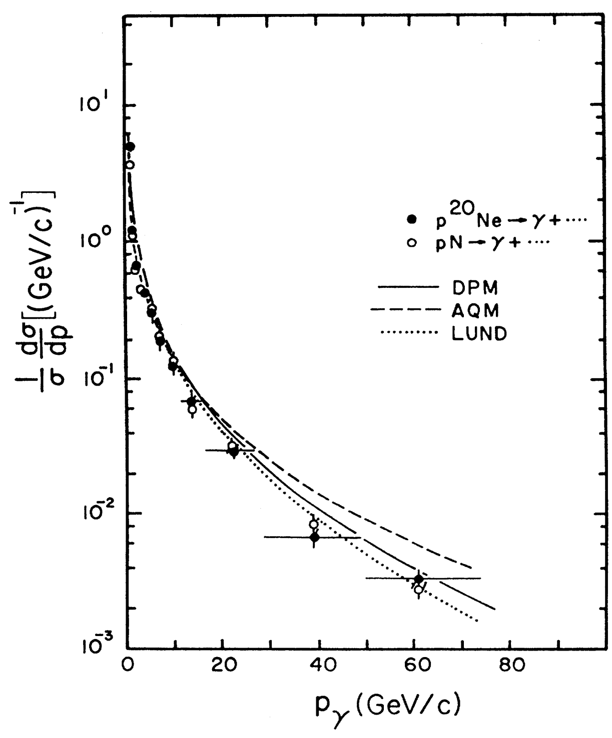


FIG. 13. The laboratory momentum distributions of $\gamma$ for the $p\,^{20}$Ne and $pN$ interactions. The curves are predictions of the discussed models for $p\,^{20}$Ne events.

In Fig. 12 we display a plot of $\langle n_\gamma \rangle$ as a function of $n_p$ for different rapidity regions for $p\,^{20}$Ne interactions. Once again we see that the correlation is weakest for $\gamma$ with $y^* > 1$, the projectile-fragmentation region. All the models predict this effect rather well. However, in the central region ($|y^*| < 1$) and the "target"-fragmentation region ($y^* > 1$), the models make very different predictions. In general, the DPM agrees best with the data.

Clearly the average $\gamma$ multiplicity ($\pi^0$, $\eta^0$ mesons) is strongly correlated with the number of secondary pions and protons (in the $p\,^{20}$Ne interactions). The main contribution to these observed correlations comes from $\gamma$'s ($\pi^0$, $\eta^0$ mesons) produced in the central and the target-fragmentation region. We also conclude that, although the AQM, LM, and the DPM quite satisfactorily reproduce the average $\gamma$ multiplicity, these models do not quantitatively describe all the correlations observed in this experiment.

## VI. $\gamma$ INCLUSIVE SPECTRA

The $\gamma$ momentum distributions in the laboratory frame for $p\,^{20}$Ne and $pN$ interactions are shown in Fig. 13. Since most $\gamma$'s are produced by the decay of $\pi^0$ mesons, the maximum value of $p_\gamma$ in the laboratory frame cannot exceed $p_\gamma^{\max} \simeq 80$ GeV [from $pp \to (p\pi^0)p$] for an incoming proton of momentum $p_0 = 300$ GeV/$c$. The curves correspond to predictions of the AQM, LM, and DPM for $p\,^{20}$Ne interactions. Most models reproduce the momentum distribution rather well, although the AQM overestimates the yield of fast $\gamma$.

A comparison of the $\gamma$ inclusive spectra for $p\,^{20}$Ne and $pN$ interactions can be seen in the rapidity distributions shown in Figs. 14(a) and 14(b), where the ratio

$$R(y) = \frac{(\sigma_{\text{in}}^{-1} d\sigma/dy^*)_{p\,\text{Ne}}}{(\sigma_{\text{in}}^{-1} d\sigma/dy^*)_{pN}}$$

is shown. There is a clear indication that $R(y) > 1$ in the target-fragmentation region. On the other hand, in the projectile-fragmentation region ($y^* \gtrsim 2$), the data indicate $R(y^*) < 1$, i.e., in the very forward direction the average $\gamma$ multiplicity of $\gamma$'s (due to $\pi^0$, $\eta^0$ mesons) may be less for $p\,^{20}$Ne than for $pN$ events. this same effect has been observed for charged particles also.[1-4] In general, the models reproduce the coarse features of the $\gamma$ rapidity spectra in $p\,^{20}$Ne interactions, although the detailed agreement is far from satisfactory.

In Fig. 15 the $\gamma$ transverse-momentum $p_\perp^2$ distribution for the $p\,^{20}$Ne and $pN$ interactions is shown. The model predictions agree well with the data, although the AQM prediction for $p\,^{20}$Ne interactions is low for the large ($p_\perp^2 \gtrsim 0.6$ GeV$^2/c^2$) transverse momentum.

In Figs. 16 and 17 we show the $\gamma$ inclusive spectra for different numbers of secondary protons. The predictions of both the AQM and DPM are similar, and closer to the experimental data, than the LM. Within the framework

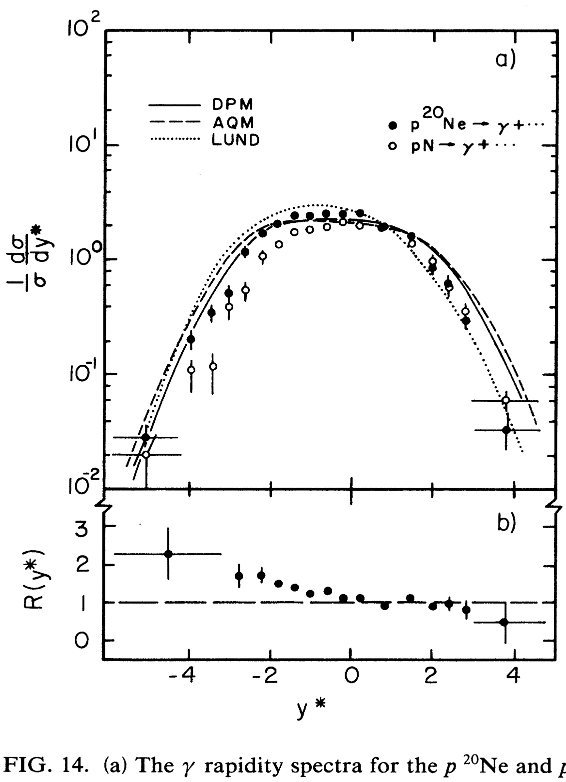


FIG. 14. (a) The $\gamma$ rapidity spectra for the $p\,^{20}$Ne and $pN$ interactions. The curves are predictions of the discussed models for the $p\,^{20}$Ne collisions. (b) The ratio of normalized $\gamma$ inclusive spectra, $R(y^*) = (\sigma_{\text{in}}^{-1} d\sigma/dy^*)_{p\,\text{Ne}} / (\sigma_{\text{in}}^{-1} d\sigma/dy^*)_{nN}$, for the $p\,^{20}$Ne and $pN$ interactions as a function of rapidity. Curves are model predictions for $p\,^{20}$Ne events.

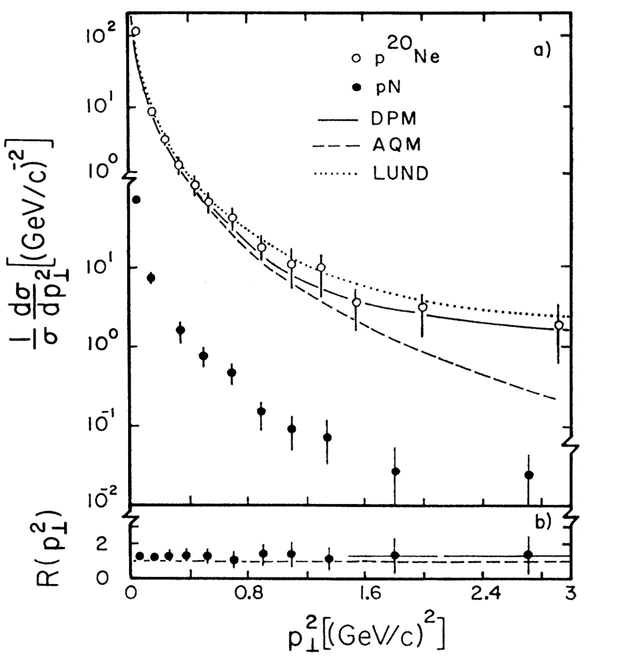


FIG. 15. (a) The $p_\perp^2$ distributions for $\gamma$ in $p\,^{20}$Ne and $pN$ interactions. The curves are model predictions for the $p\,^{20}$Ne interactions. (b) The ratio of normalized $\gamma$ $p_\perp^2$ spectra, $R(p_\perp^2) = (\sigma_{\text{in}}^{-1} d\sigma/dp_\perp^2)_{p\,\text{Ne}} / (\sigma_{\text{in}}^{-1} d\sigma/dp_\perp^2)_{pN}$ for $p\,^{20}$Ne and $pN$ interactions.

of the Lund model, the Monte Carlo calculations show that the probability for the final state to have five or more protons within our visible range ($0.12 \le p_p \le 1.2$ GeV/$c$) is less than $5 \times 10^{-5}$.

Finally, in Figs. 18 and 19 we compare inclusive rapidity and transverse momentum distributions for $\gamma$, $\pi^0$, and $\eta^0$ mesons in $p\,^{20}$Ne interactions. Data for the $\pi^0$ and $\eta^0$ mesons were obtained from the $y^*$ and $p_\perp^2$ distributions of $\gamma\gamma$ systems with masses

$$0.90 \le M(\gamma\gamma) \le 0.180 \text{ GeV}$$

($\pi^0$ meson) and

$$0.500 \le M(\gamma\gamma) \le 0.600 \text{ GeV}$$

($\eta^0$ meson). The background $y^*$ and $p_\perp^2$ distributions were obtained by randomly mixing $\gamma$'s from different $p\,^{20}$Ne events and were normalized to the corresponding background in the $M(\gamma\gamma)$ spectrum at the $\pi^0$ and $\eta^0$ mass regions, respectively.

At large values of $p_\perp^2$, the absolute yields of $\pi^0$ and $\eta^0$ mesons become closer. A similar trend is observed in $pp$ interactions.[14,18,22–24] In addition, in the target-fragmentation region the $\pi^0$ and $\eta^0$ yields become comparable.

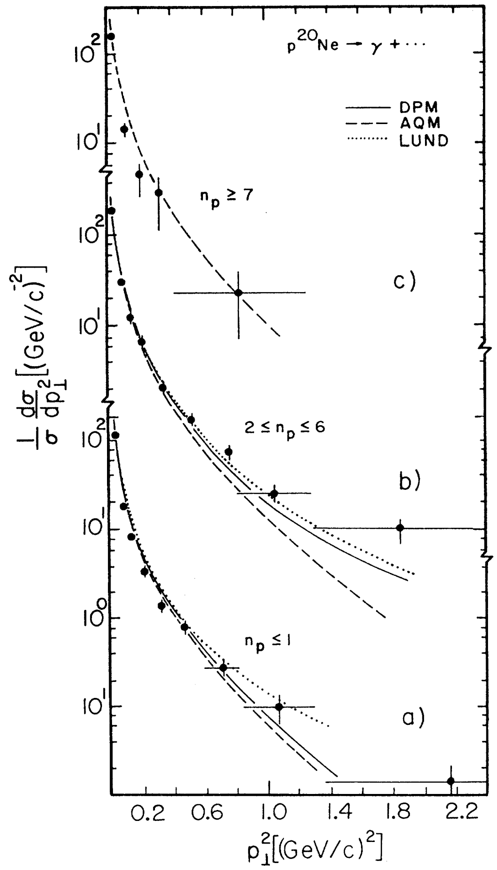


FIG. 17. The $\gamma$ $p_\perp^2$ spectra for $p\,^{20}$Ne collisions with a fixed number of protons in final state: (a) $n_p \le 1$, (b) $2 \le n_p \le 6$, and (c) $n_p \le 7$.

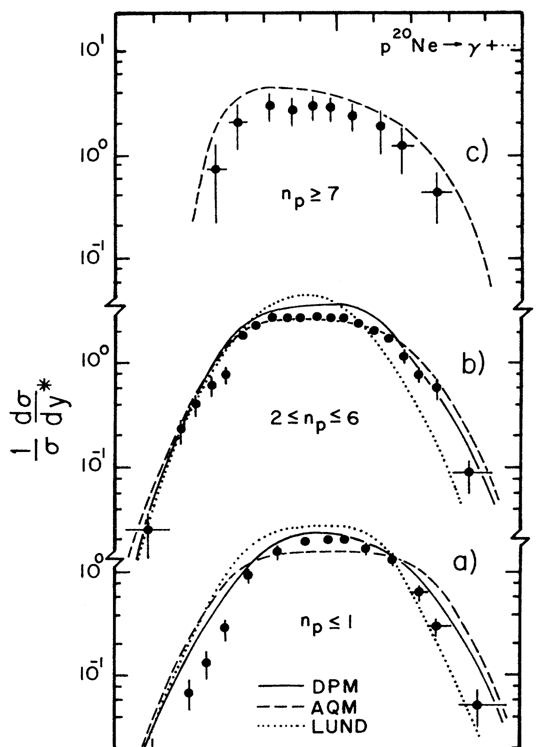


FIG. 16. The $\gamma$ rapidity spectra for the $p\,^{20}$Ne interactions with a fixed number of protons in the final state: (a) $n_p \le 1$, (b) $2 \le n_p \le 6$, and (c) $n_p \ge 7$. The curves are model predictions.

## VII. CORRELATIONS BETWEEN TRANSVERSE AND LONGITUDINAL MOMENTA OF $\gamma$ QUANTA

As shown in the previous section, the transverse-momentum distributions of $\gamma$ quanta in the $p\,^{20}$Ne and $pN$ interactions have similar shapes in the interval $0 \le p_\perp^2 \lesssim 3$ (GeV/$c$)$^2$. As a result, the average $p_\perp$ coincides

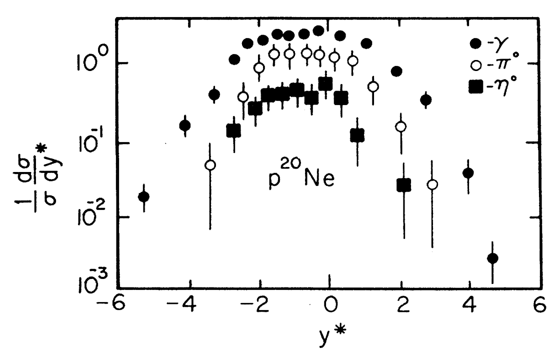


FIG. 18. The rapidity spectra for $\gamma$, $\pi^0$, and $\eta^0$ mesons in $p\,^{20}$Ne interactions.

for both types of interactions:

$$\langle p_{\perp\gamma}\rangle_{p\,\mathrm{Ne}}=(180\pm4)\ \mathrm{MeV}/c$$

in $p\,^{20}$Ne and

$$\langle p_{\perp\gamma}\rangle_{pN}=(178\pm5)\ \mathrm{MeV}/c$$

in the $pN$ interactions.

However, it is interesting to look at the $p_\perp$ distributions in different kinematical regions. In Fig. 20 the average $\gamma$ transverse momentum is shown as a function of the Feynman variable $x=2p_\parallel^*/\sqrt{s}$ for $p\,^{20}$Ne interactions with the number of secondary protons $n_p\le1$ (i.e., mostly interactions with quasifree nucleons) and $n_p\ge2$. The "seagull" effect is apparent in both cases, but the $\langle p_\perp\rangle$ dependence on $x$ is asymmetric for events with $n_p\ge2$. For $x\lesssim-0.05$, the $\langle p_\perp\rangle_{n_p\ge2}$ is smaller than $\langle p_\perp\rangle_{n_p\le1}$; for $x\gtrsim0.05$ they are roughly equal. This difference, which is as large as 20%, cannot be explained either by the Lund model or the additive quark model as shown in Fig. 20.

The $\langle p_\perp\rangle$ difference for $\gamma$ with $x\lesssim-0.1$ can be caused by a low-energy cascading of slow hadrons in a nucleus. As the number of protons in the final state increases (implying an increase of $\langle\nu\rangle$), the average transverse momenta of hadrons should decrease with $n_p$ due to conservation of energy and momentum. In Fig. 21(a) we show $\langle p_\perp\rangle$ as a function of $n_p$ for $\gamma$ with $x\le-0.05$. Qualitatively, the observed decrease of $\langle p_\perp\rangle$ with $n_p$ is explained by the AQM but not by the LM, which neglects the rescattering of slow hadrons.

This low-energy cascading in the target-fragmentation region should cause an increase in the dispersion of the $p_\perp$ distribution as $n_p$ increases. Our data agree with this: for $\gamma$'s with $x<-0.05$, the dispersion of the $p_\perp$ distribution is $D(p_\perp)=0.06\pm0.01$ for events with $n_p\le1$, and $D(p_\perp)=0.09\pm0.01$ for events with $n_p\ge2$.

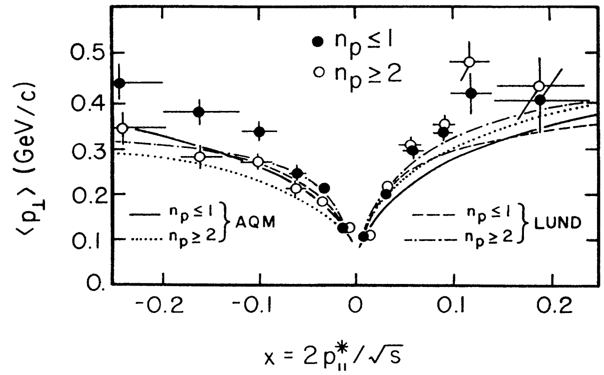


FIG. 20. The $\langle p_\perp\rangle$ vs Feynman $x$ for $\gamma$ in $p\,^{20}$Ne interactions with the number of protons $n_p\le1$ (solid circles) and $n_p\ge2$ (open circles). The predictions of the AQM and LM are shown.

In the central region ($|x|\lesssim0.05$), there are several alternative processes due to a finite "formation" time of hadrons. In this case, since hadrons are relatively fast in the laboratory frame, one can expect the absence of noticeable correlations. Data in Fig. 21(b) show that, for $\gamma$ with $|x|\le0.05$, the $\langle p_\perp\rangle$ does not depend on the multiplicity of slow protons in the final state. This is also in agreement with the predictions of the LM and AQM.

The most interesting dependence of $\langle p_\perp\rangle$ on $n_p$ occurs for fast $\gamma$'s ($x>0.05$), which originate mainly from decays of fast $\pi^0$ mesons produced due to projectile fragmentation. As one can see from Fig. 21(c), $\langle p_\perp\rangle$ for these $\gamma$'s may increase with $n_p$ for $n_p\lesssim3$ and then decreases as $n_p$ increases further. Qualitatively, such behavior does not contradict the AQM, although a different mechanism may be responsible. For example, successive

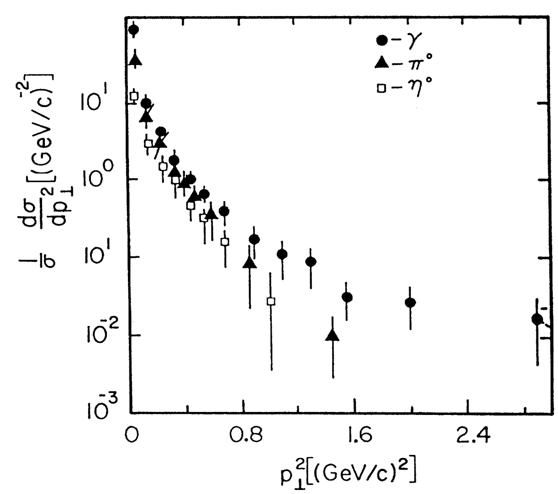


FIG. 19. The $p_\perp^2$ spectra of $\gamma$, $\pi^0$, and $\eta^0$ mesons in $p\,^{20}$Ne interactions.

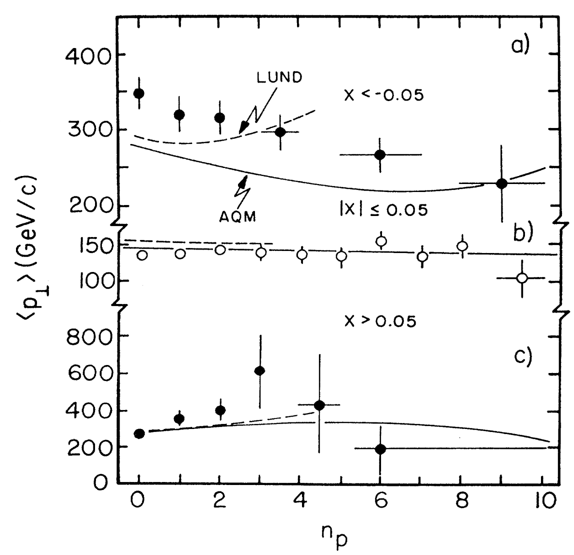


FIG. 21. The average $\gamma$ transverse momentum as a function of the number of protons for $p\,^{20}$Ne interactions with a fixed range of Feynman $x$.

rescatterings of the incoming hadron (or some excited hadronic system connected with projectile) on nucleons inside a nucleus can cause the appearance of additional transverse momentum for hadrons produced from projectile fragmentation. In this case, one could observe an increase of $\langle p_\perp \rangle$ up to some value of $n_p$, then a leveling off at higher values of $n_p$ because of the finite number of nucleons in a nucleus. This would also imply that an increase of $\langle p_\perp \rangle$ with $n_p$ should be observed to larger values of $n_p$ for heavier nuclei.

## VIII. CONCLUSION

In this paper we have presented data on the inclusive production of $\gamma$ in $p\,^{20}$Ne and $pN$ interactions at 300 GeV/$c$. The average multiplicities for $\gamma$, $\pi^0$, and $\eta^0$ mesons in the $p\,^2$Ne interactions are $11.43\pm0.23$, $4.91\pm0.52$, and $1.47\pm0.33$, respectively. The ratio of $\langle n_\gamma \rangle$ for $p\,^{20}$Ne interactions compared to $pN$ collisions is $1.48\pm0.05$, very similar to the corresponding ratio for $\langle n_- \rangle$ of $1.47\pm0.23$. $\eta^0$ production in the $p\,^{20}$Ne interactions is measured to be $0.29\pm0.07$ of $\pi^0$ production, compared to $0.05\pm0.04$ for $pN$ interactions. $\Sigma^0$ production accounts for only $(0.65\pm0.16)\%$ of all $\gamma$. No $\eta'(958)$ production is observed. Altogether, $\pi^0$, $\eta^0$, and $\Sigma^0$ productions account for 99.5% of the observed $\gamma$.

We have observed strong correlations between the average $\gamma$ multiplicity and the number of charged particles; these correlations are strongest for $\gamma$ produced in the central and target-fragmentation regions. We have analyzed the inclusive spectra of secondary $\gamma$, $\pi^0$, and $\eta^0$ mesons and found an indication of low-energy cascading as well as rescattering of fast particles in the projectile-fragmentation region.

The comparison of this experimental data with Monte Carlo calculations using the additive quark model, the Lund model, and the dual parton model shows that these models, which reproduce many of the gross features of the data, do not quantitatively describe all the properties of inclusive $\gamma$ production.

## ACKNOWLEDGMENTS

We thank E. Stenlund and V. V. Uzhinski for valuable discussions of some model calculation aspects. We also wish to express our sincere appreciation to the scanning and measuring staffs at Tashkent and Wisconsin for their efforts and we acknowledge the fine efforts on the part of the 30-in. bubble-chamber crew at Fermilab. We gratefully acknowledge the efforts of Professor A. Erwin and other members of the Wisconsin group before and during the data-taking phase of the experiment. Our thanks go also to L. Voyvodic for help and encouragement. One of us (B.S.Y.) thanks Professor H. J. Lubatti for fruitful discussions and hospitality during a stay at the University of Washington.

---

*Present address: Institute of Nuclear Physics, The Uzbek Academy of Sciences, Ulugbek, Tashkent 702132, U.S.S.R.

[1] B. B. Levchenko and N. N. Nikolaev, Yad. Fiz. **37**, 1016 (1983) [Sov. J. Nucl. Phys. **37**, 602 (1983)].

[2] B. Andersson *et al.*, Phys. Rep. C **97**, 1 (1983); B. Andersson *et al.*, Nucl. Phys. **281B**, 289 (1987).

[3] A. Capella and J. Tran Thanh Van, Z. Phys. C **10**, 210 (1981); A. Capella and J. Tran Thanh Van, *ibid.* **33**, 541 (1987); J. Ranft and S. Ritter, *ibid.* **27**, 413 (1985); N. S. Amelin *et al.*, Yad. Fiz. **51**, 1730 (1990) [Sov. J. Nucl. Phys. **51**, 1093 (1990)].

[4] A. M. Zadoroshni *et al.*, Yad. Fiz. **39**, 1155 (1984) [Sov. J. Nucl. Phys. **39**, 729 (1984)]; Joint Institute for Nuclear Research Report No. P2-86-381, 1986 (unpublished).

[5] M. I. Strikman and L. L. Frankfurt, Phys. Rep. **76**, 215 (1981).

[6] S. A. Azimov *et al.*, Phys. Rev. D **23**, 2512 (1981).

[7] Kh.Kh. Artykov *et al.*, Yad. Fiz. **43**, 1472 (1986) [Sov. J. Nucl. Phys. **43**, 949 (1986)].

[8] S. A. Azimov *et al.*, Physico-Technical Institute Report No. 29-85-FVE, 1985, in Russian (unpublished).

[9] A. Sheng *et al.*, Phys. Rev. D **11**, 1733 (1975).

[10] F. T. Dao *et al.*, Phys. Rev. Lett. **30**, 1151 (1973).

[11] Y. S. Barashenkov and V. D. Toneev, *Interactions of High Energy Particles and Nuclei with Nuclei* (Atomizdat, Moscow, 1972), in Russian.

[12] Particle Data Group, M. Aguilar-Benitez *et al.*, Phys. Lett. B **204**, 1 (1988).

[13] M. Aguilar-Benitez *et al.*, Z. Phys. C **34**, 419 (1987).

[14] A. V. Batunin *et al.*, in *Physics at Future Accelerators,* proceedings of the Xth Warsaw Symposium, Kazimierz, Poland, 1987, edited by Z. Ajduk (Warsaw University, Warsaw, 1987), p. 187.

[15] M. Diakonou *et al.*, Phys. Lett. **87B**, 292 (1979); M. Diakonou *et al.*, *ibid.* **91B**, 296 (1980).

[16] A. L. Angelis *et al.*, Phys. Lett. **94B**, 106 (1980).

[17] T. Akesson *et al.*, Phys. Lett. B **178**, 447 (1986).

[18] B. Andersson *et al.*, Phys. Lett. **73B**, 343 (1978).

[19] S. A. Azimov *et al.*, Yad. Fiz. **33**, 1562 (1981) [Sov. J. Nucl. Phys. **33**, 841 (1981)].

[20] B. S. Yuldashev *et al.*, in *Multiparticle Dynamics,* proceedings of the XVIII International Symposium, Tashkent, USSR, 1987, edited by I. Dremin and K. Gulamov (World-Scientific, Singapore, 1988), p. 261.

[21] M. L. Allaberdin *et al.*, Yad. Fiz. **39**, 662 (1984) [Sov. J. Nucl. Phys. **39**, 420 (1984)].

[22] J. Antille *et al.*, Phys. Lett. B **194**, 568 (1987).

[23] T. Akesson *et al.*, Phys. Lett. **158B**, 282 (1985).

[24] T. Akesson *et al.*, Z. Phys. C **18**, 5 (1983).